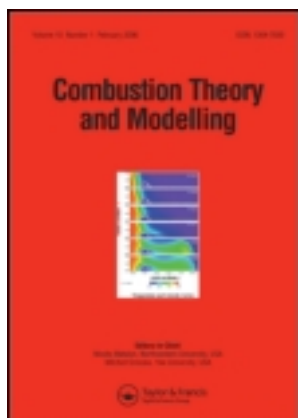


This article was downloaded by: [Cornell University]

On: 03 January 2012, At: 10:20

Publisher: Taylor & Francis

Informa Ltd Registered in England and Wales Registered Number: 1072954 Registered office: Mortimer House, 37-41 Mortimer Street, London W1T 3JH, UK



## Combustion Theory and Modelling

Publication details, including instructions for authors and subscription information:

<http://www.tandfonline.com/loi/tctm20>

### Reduced description of reactive flows with tabulation of chemistry

Zhuyin Ren<sup>a</sup>, Graham M. Goldin<sup>a</sup>, Varun Hiremath<sup>b</sup> & Stephen B. Pope<sup>b</sup>

<sup>a</sup> ANSYS, Inc., 10 Cavendish Court, Lebanon, NH, 03766, USA

<sup>b</sup> Sibley School of Mechanical & Aerospace Engineering, Cornell University, Ithaca, NY, 14853, USA

Available online: 19 Jul 2011

To cite this article: Zhuyin Ren, Graham M. Goldin, Varun Hiremath & Stephen B. Pope (2011): Reduced description of reactive flows with tabulation of chemistry, *Combustion Theory and Modelling*, 15:6, 827-848

To link to this article: <http://dx.doi.org/10.1080/13647830.2011.574156>

PLEASE SCROLL DOWN FOR ARTICLE

Full terms and conditions of use: <http://www.tandfonline.com/page/terms-and-conditions>

This article may be used for research, teaching, and private study purposes. Any substantial or systematic reproduction, redistribution, reselling, loan, sub-licensing, systematic supply, or distribution in any form to anyone is expressly forbidden.

The publisher does not give any warranty express or implied or make any representation that the contents will be complete or accurate or up to date. The accuracy of any instructions, formulae, and drug doses should be independently verified with primary sources. The publisher shall not be liable for any loss, actions, claims, proceedings, demand, or costs or damages whatsoever or howsoever caused arising directly or indirectly in connection with or arising out of the use of this material.

## Reduced description of reactive flows with tabulation of chemistry

Zhuyin Ren<sup>a\*</sup>, Graham M. Goldin<sup>a</sup>, Varun Hiremath<sup>b</sup> and Stephen B. Pope<sup>b</sup>

<sup>a</sup>ANSYS, Inc., 10 Cavendish Court, Lebanon, NH, 03766, USA; <sup>b</sup>Sibley School of Mechanical & Aerospace Engineering, Cornell University, Ithaca, NY 14853, USA

(Received 30 November 2010; final version received 7 March 2011)

The direct use of large chemical mechanisms in multi-dimensional Computational Fluid Dynamics (CFD) is computationally expensive due to the large number of chemical species and the wide range of chemical time scales involved. To meet this challenge, a reduced description of reactive flows in combination with chemistry tabulation is proposed to effectively reduce the computational cost. In the reduced description, the species are partitioned into represented species and unrepresented species; the reactive system is described in terms of a smaller number of represented species instead of the full set of chemical species in the mechanism; and the evolution equations are solved only for the represented species. When required, the unrepresented species are reconstructed assuming that they are in constrained chemical equilibrium. In situ adaptive tabulation (ISAT) is employed to speed the chemistry calculation through tabulating information of the reduced system. The proposed dimension-reduction / tabulation methodology determines and tabulates *in situ* the necessary information of the  $n_r$ -dimensional reduced system based on the  $n_s$ -species detailed mechanism. Compared to the full description with ISAT, the reduced descriptions achieve additional computational speed-up by solving fewer transport equations and faster ISAT retrieving. The approach is validated in both a methane/air premixed flame and a methane/air non-premixed flame. With the GRI 1.2 mechanism consisting of 31 species, the reduced descriptions (with 12 to 16 represented species) achieve a speed-up factor of up to three compared to the full description with ISAT, with a relatively moderate decrease in accuracy compared to the full description.

**Keywords:** reduced description of reactive flows; dimension reduction; tabulation; constrained equilibrium; operator splitting

### 1. Introduction

Realistic modelling of chemically reactive flows involves a large number of chemical species, which participate in tens to thousands of chemical reactions occurring simultaneously within a complex flow field [1]. For example, the detailed mechanism for iso-octane [2] contains more than 800 species that participate in more than 3000 reactions. Currently, it is computationally expensive to directly incorporate detailed chemical kinetics in multi-dimensional Computational Fluid Dynamics (CFD) due principally to the large number of species involved and the wide range of chemical time scales present, although its use in CFD is essential for a reliable prediction of ignition and extinction phenomena, and pollutants such as CO and NO<sub>x</sub>.

---

\*Corresponding author. Email: ZhuyinRen@gmail.com

In the past decade, significant progress has been made in methodologies and algorithms that rationally reduce the computational burden imposed by the use of detailed chemical kinetics in CFD calculations of reactive flows [1, 3–29]. Among the available techniques, three frequently used in the literature are: the development of skeletal mechanisms from large detailed mechanisms by the elimination of inconsequential species and reactions [9–11]; dimension-reduction techniques [12–27]; and storage/retrieval methodologies such as in situ adaptive tabulation (ISAT) [28–29]. Note that the above three techniques can be used in combination to speed up the chemistry calculation in CFD. As demonstrated in [17, 30], the computational cost of using detailed chemical kinetics in CFD is dramatically reduced by exploiting, in combination, techniques of dimension reduction and storage retrieval.

The purpose of dimension reduction is to describe reactive systems using a smaller number of reduced compositions while reproducing the characteristics of the full description in which the full set of chemical species in the detailed kinetics is employed. For example, the quasi-steady-state assumption (QSSA) method [12–14] partitions the species into ‘major’ species and ‘minor’ species. The minor species, typically those with fast consumption reactions, are assumed to be in quasi-steady state. Each of the resulting algebraic equations can be used to eliminate one minor species from the governing equations. In the reduced description, reactive systems are described in terms of only the major species. The possibility of a reduced description of reactive flows by dimension-reduction methods is based on the fact that, in general, the range of time scales for chemical kinetic processes is much larger than that for transport processes [22]. Due to the fast chemical time scales, compositions in reactive flows quickly relax toward a low-dimensional manifold in the full composition space. Therefore reactive systems can be well described with a smaller number of parameterisation variables.

As pointed out in [31], dimension reduction can be approached from the perspective of ‘species reconstruction’, recognising that the reduced description given by most dimension reduction methods is in terms of specified represented/major species, and then when necessary there is a species reconstruction procedure by which the remaining unrepresented/minor species are determined. For example, in the QSSA reduced description, only when evaluating the rate-of-change of the major species, the minor species are reconstructed based on a set of algebraic equations resulting from QSSA approximations. In this work, from the species reconstruction perspective, we develop a general, combined dimension reduction/tabulation methodology for the reduced description of reactive flows. In the reduced description, the full set of  $n_s$  chemical species involved in the detailed chemical kinetics are partitioned into ‘represented species’ and ‘unrepresented species’; the reactive flow calculation is performed in terms of a small number of  $n_r$  reduced compositions, which are the represented species and the elements in the unrepresented species. With a splitting scheme, chemical reaction is separated from other physical processes into a reaction fractional step. Given the reduced composition before reaction, the task in this step is to determine the corresponding reduced composition after (adiabatic, isobaric) reaction has occurred for a time-step interval. The ISAT algorithm, a storage/retrieval technique, tabulates the reduced composition information before and after reaction, so that, given the reduced composition before the reaction fractional step, the corresponding values after reaction can be retrieved from the table efficiently (when possible within acceptable accuracy). Only when needed, ISAT adds new entries of the reduced compositions to the table by invoking the species reconstruction procedure and evaluating the exact mapping in the full composition space together with the detailed mechanism (as described later in Section 2.1). In other words, the dimension-reduction/tabulation methodology determines and tabulates, in situ, the

necessary information of the  $n_r$ -dimensional reduced system. The unrepresented species are needed to evaluate the reaction mapping of the reduced composition, and when required they are reconstructed by assuming that they are in constrained chemical equilibrium.

The outline of the remainder of the paper is as follows. In Section 2, the reduced description of reactive flows with species reconstruction is described. Then in Section 3, tabulation of the combustion chemistry using ISAT for the reduced description is formulated. The implementation of the reduced description in CFD is discussed in Section 4. Numerical tests are reported in Section 5. Section 6 provides a discussion and conclusions.

## 2. Reduced description of reactive flows

With the detailed mechanism consisting of  $n_s$  chemical species composed on  $n_e$  elements, let  $\mathbf{z}$ , a vector of length  $n_s$ , denote the species specific moles,  $p$  denote the pressure, and  $h$  denote the mixture enthalpy. In the full description, the thermo-chemical state of the reactive system is represented by  $\Phi(\mathbf{x}, t) = \{\mathbf{z}(\mathbf{x}, t); h(\mathbf{x}, t); p(\mathbf{x}, t)\}$ , which is generally a function of time and space. Another often used representation is  $\{\mathbf{z}(\mathbf{x}, t); h_s(\mathbf{x}, t); p(\mathbf{x}, t)\}$ , where  $h_s$  is the mixture sensible enthalpy. The species evolve according to the set of  $n_s$  partial differential equations (PDEs)

$$\frac{\partial \mathbf{z}}{\partial t} + v_i \frac{\partial \mathbf{z}}{\partial x_i} = \mathbf{D}\{\mathbf{z}(\mathbf{x}, t)\} + \mathbf{S}(\mathbf{z}(\mathbf{x}, t)) \quad (1)$$

where  $\mathbf{S}$  denotes the rate of change due to chemical reactions given by the provided detailed chemical kinetics. The spatial transport includes the convective contribution ( $v_i \frac{\partial \mathbf{z}}{\partial x_i}$ , where  $\mathbf{v}(\mathbf{x}, t)$  is the velocity field) and the diffusive contribution  $\mathbf{D}$ . In calculations of reactive flows, one simplified model widely used for diffusion is

$$\mathbf{D}\{\mathbf{z}\} = \frac{1}{\rho} \nabla \cdot (\rho \mathbf{\Gamma} \nabla \mathbf{z}) \quad (2)$$

where  $\rho$  is mixture density and  $\mathbf{\Gamma}$  is a diagonal matrix with the diagonal components  $\Gamma_1, \Gamma_2, \dots, \Gamma_{n_s}$  being the mixture-averaged species diffusivities, which are usually functions of  $\mathbf{z}$ . It is worth mentioning that the methodology and results presented in this work do not depend on this model.

In the reduced description, species are decomposed as  $\mathbf{z} = \{\mathbf{z}^r, \mathbf{z}^u\}$ , where  $\mathbf{z}^r$  is an  $n_{rs}$  vector of represented species, and  $\mathbf{z}^u$  is an  $n_{us}$ -vector of unrepresented species (with  $n_{rs} + n_{us} = n_s$  and  $n_{rs} < n_s - n_e$ ). The ‘reduced representation’ of the species used in the reduced description is  $\mathbf{r} \equiv \{\mathbf{z}^r, \mathbf{z}^{u,e}\}$ , where  $\mathbf{z}^{u,e}$  is an  $n_e$ -vector giving the specific moles of the elements in the unrepresented species. Thus  $\mathbf{r}$  is a vector of length  $n_r = n_{rs} + n_e$ , and the dimension of the system is reduced from  $n_s$  to  $n_r$ . This dimension reduction process can be written as

$$\mathbf{r} = \mathbf{B}^T \mathbf{z} \quad (3)$$

where  $\mathbf{B}$  is a known constant  $n_s \times n_r$  matrix. For example, if the species in a mechanism are ordered such that the represented species are first in the ordering,  $\mathbf{B}$  is given by

$$\mathbf{B} = \begin{bmatrix} \mathbf{I} & \mathbf{0} \\ \mathbf{0} & \mathbf{E}^u \end{bmatrix} \quad (4)$$

where  $\mathbf{I}$  is an  $n_{rs} \times n_{rs}$  identity matrix and  $\mathbf{E}^u$  ( $n_{us} \times n_e$ ) is the elemental matrix for the unrepresented species, with the component  $E^u_{ij}$  indicating the number of atoms of element  $j$  in a molecule of species  $i$ . That is, if a component of  $\mathbf{r}$  is a specified represented species, then the corresponding column of  $\mathbf{B}$  is a unit vector consisting of a single entry (unity) in the row corresponding to the represented species.

It is worth mentioning that this reduced representation is similar to those used in intrinsic low-dimensional manifolds (ILDm) [22], the rate-controlled constrained equilibrium method (RCCE) [15–20] and the invariant constrained equilibrium edge pre-image curve method (ICE-PIC) [24], in the sense that both represented species and elements are needed in the reduced description. In contrast, the QSSA reduced description needs only the represented (or major) species since the elements are fully represented by the represented species [32].

In this work, with assigned thermal and transport properties, the elements in the unrepresented species  $\mathbf{z}^{u,e}$  are treated as ‘notional species’ in the reduced description with corresponding PDEs governing their evolution. The thermo-chemical state of the reactive system is represented by  $\tilde{\mathbf{r}}(\mathbf{x}, t) = \{\mathbf{r}(\mathbf{x}, t); h(\mathbf{x}, t); p(\mathbf{x}, t)\}$ . (Another feasible reduced representation is  $\{\mathbf{r}(\mathbf{x}, t); h_s(\mathbf{x}, t); p(\mathbf{x}, t)\}$ , where the mixture sensible enthalpy is redefined based on the reduced composition  $\mathbf{r}$ .) By pre-multiplying Equation (1) with matrix  $\mathbf{B}^T$ , the evolution equations of the  $n_r$  reduced composition variables can be obtained as

$$\frac{\partial \mathbf{r}}{\partial t} + v_i \frac{\partial \mathbf{r}}{\partial x_i} = \mathbf{B}^T \mathbf{D}\{\mathbf{z}(\mathbf{x}, t)\} + \mathbf{B}^T \mathbf{S}(\mathbf{z}(\mathbf{x}, t)) \approx \mathbf{D}\{\mathbf{r}(\mathbf{x}, t)\} + \mathbf{B}^T \mathbf{S}(\mathbf{z}(\mathbf{x}, t)) \quad (5)$$

where the term  $\mathbf{B}^T \mathbf{S}$  denotes the rate of change of the reduced composition due to chemical reactions, and the second step follows with the assumption that the diffusion term is linear with respect to composition. For example, with the widely used simplified model (see Equation (2)), by neglecting any nonlinearity in species diffusivity, the diffusion contribution in the reduced description can be written as

$$\mathbf{D}\{\mathbf{r}\} = \frac{1}{\rho} \nabla \cdot (\rho \mathbf{\Gamma} \nabla \mathbf{r}) \quad (6)$$

where  $\rho$  is mixture density and  $\mathbf{\Gamma}$  is a diagonal matrix with the diagonal components  $\Gamma_1, \Gamma_2, \dots, \Gamma_{n_r}$  being the mixture-averaged species diffusivities. Notice that the transient and advection terms in Equation (5) are exact. The diffusion term invokes the linearity approximations for transport properties and also approximations for the transport properties of the ‘notional’ species. The effects of these approximations are small as demonstrated below even for laminar flames. Hence the major challenge in the reduced description is to model the effect of chemical reactions on the reduced composition, i.e., the effect of the term  $\mathbf{B}^T \mathbf{S}$ .

### 2.1 Species reconstruction using constrained equilibrium

The modelling of the effect of chemical reactions on the reduced composition is addressed through species reconstruction and the evaluation of reaction mapping in the full composition space. That is, given  $\mathbf{r}$  (together with  $h$  and  $p$ ), we define a full composition  $\mathbf{z}$ , which is regarded to be the one occurring in reactive flows. Once  $\mathbf{z}$  is determined, with the given detailed chemical kinetics, the full set of species in the mechanism (together with the

energy variable) is integrated for a reaction time step to obtain the reaction mapping of the full composition, from which the reaction mapping of the reduced composition (i.e., the reduced composition after reaction) is extracted.

Several dimension reduction methods such as ILDM, RCCE and ICE-PIC can be used to reconstruct the full composition. In this work, we take  $\mathbf{z}$  to be  $\mathbf{z}^{\text{CE}}(\mathbf{r}, h, p)$ , which is the constrained equilibrium (maximum-entropy) composition, as used in the RCCE method, [15–17]. This is readily computed using the constrained equilibrium code CEQ [33]. Briefly stated, with fixed pressure and mixture enthalpy, the constrained equilibrium composition is defined to be that which maximises the mixture entropy subject to the constraints that the specific moles of the represented species  $\mathbf{z}^r$  and the moles of the elements in the unrepresented species  $\mathbf{z}^{u,e}$  are held fixed. Given a realisable reduced composition, the constrained equilibrium (maximum-entropy) composition is guaranteed to exist and to be unique [33]. As revealed by previous works [17–20], the accuracy of the reduced description depends on the quality of the reconstructed full composition and therefore the selection of the represented species. At the present stage of development of the methodology, the represented species are manually specified, although other approaches are available such as the greedy algorithm [34]. Boundary and initial species are included in the represented species list. Species of interest, especially slow-forming species that are far from chemical equilibrium, such as pollutants, should also be included. Intermediate species that occur in large mass fractions relative to the fuel and oxidiser species are included, as well as species important in the chemical pathway. For example, for methane combustion in air,  $H$  and  $OH$  are included as represented species since these are important intermediate radicals. In Section 5, the effect of different selections of represented species on reduced description is studied.

The reduced description described above is implemented in a CFD solver as follows:

- The CFD solver solves the transport equations for the reduced composition that consists of the represented species, the unrepresented elements and mixture enthalpy, i.e.,  $\tilde{\mathbf{r}} = \{\mathbf{r}; h\}$ . The unrepresented elements are treated as ‘notional species’ with assigned thermal and transport properties.
- With an operator splitting scheme, chemical reactions are separated from other physical processes into an adiabatic, isobaric reaction fractional step. Given the reduced composition  $\tilde{\mathbf{r}}(t)$  at time  $t$ , the task in this reaction fractional step is to determine the reaction mapping  $\mathbf{R}(\tilde{\mathbf{r}}(t))$ , i.e., the reduced composition  $\tilde{\mathbf{r}}(t + \Delta t)$  after (adiabatic, isobaric) reaction has occurred for the time-step interval  $\Delta t$ . (Since the governing ordinary differential equations (ODEs) for chemical reactions are autonomous, the value of  $t$  is immaterial, and without loss of generality we can set  $t = 0$ .)
- In the reaction fractional step, the unrepresented species in a cell (or grid node or particle) before reaction are first reconstructed by assuming that they are in constrained chemical equilibrium at the cell pressure and enthalpy, subject to the constraints of the represented species and the unrepresented elements. At the end of species reconstruction, the concentration of all the species in the full mechanism before reaction  $\mathbf{z}(0) \equiv \mathbf{z}^{\text{CE}}(\tilde{\mathbf{r}}(0))$  is available.
- Next, the full set of species in the mechanism (together with the energy variable) is integrated for a reaction time step according to

$$\frac{d\mathbf{z}}{dt} = \mathbf{S}(\mathbf{z}) \quad (7)$$

where rate-of-change  $\mathbf{S}$  is given by detailed chemical kinetics. After the reaction fractional step, one has the reaction mappings (i.e., the composition after reaction) of all the species,  $\mathbf{z}(\Delta t)$ , from which the reaction mappings of the reduced composition  $\mathbf{r}(\Delta t)$  can be extracted with Equation (3).

The implementation used is essentially equivalent to that described above, except that, as now described, ISAT is used to avoid the expensive ODE integration (Equation (7)). Note that the proposed reduced description can be straightforwardly adapted to employ other methods such as ILDM and ICE-PIC for reconstructing unrepresented species in the reaction fractional step.

### 3. Tabulation of combustion chemistry using ISAT

Notice that in the reduced description, the full set of species in the detailed mechanism is integrated during the reaction fractional step, which is computationally expensive. Its advantage lies in coupling with ISAT, which is employed to accelerate the determination of the reduced composition after reaction.

The ISAT algorithm introduced by Pope [28, 29] is a storage and retrieval method. Briefly stated, ISAT is used to tabulate a function  $\mathbf{f}(\mathbf{x})$ , where  $\mathbf{f}$  and  $\mathbf{x}$  are vectors of length  $n_f$  and  $n_x$ , respectively. Table entries are referred to as leaves (since in the original algorithm they are leaves of a binary tree). The  $n$ -th leaf includes:  $\mathbf{x}^{(n)}$ ; the function value  $\mathbf{f}^{(n)} = \mathbf{f}(\mathbf{x}^{(n)})$ ; and the  $n_f \times n_x$  gradient matrix  $\mathbf{A}^{(n)}$ , which has components  $A_{ij} = \partial f_i / \partial x_j$ . This matrix is used to construct the linear approximation employed in ISAT. Given a query,  $\mathbf{x}^q$ , the retrieval (i.e., the linear approximation to  $\mathbf{f}(\mathbf{x}^q)$ ) based on the  $n$ -th leaf (if it is within the user-specified error tolerance) is defined as

$$\mathbf{f}^{l,n}(\mathbf{x}^q) = \mathbf{f}(\mathbf{x}^{(n)}) + \mathbf{A}^{(n)}(\mathbf{x}^q - \mathbf{x}^{(n)}) \quad (8)$$

ISAT has been widely used to efficiently incorporate reduced or detailed chemical mechanisms in CFD calculations of turbulent reactive flows. In these applications,  $\mathbf{x}$  consists of the thermo-chemical state of a computational particle/cell at the beginning of the reaction time step (of duration  $\Delta t$ ); and  $\mathbf{f}$  represents the composition at the end of the step (resulting from adiabatic, isobaric reaction). Evaluating  $\mathbf{f}(\mathbf{x})$  involves solving a stiff set of  $n_f$  ODEs for a time  $\Delta t$  (see Equation (7)). By tabulating useful information in binary trees called ISAT tables and reusing it, ISAT can yield an accurate approximation with an up to 1000-fold speed-up.

When ISAT is employed to tabulate combustion chemistry in the reduced description, the CFD code – be it direct numerical simulation (DNS), large-eddy simulation (LES) or a probability density function (PDF) method – employs a reduced representation  $\tilde{\mathbf{r}} = \{\mathbf{r}; h\}$ . With an operator splitting scheme, chemical reaction process is separated into an adiabatic, isobaric reaction fractional step. The task in this step is to determine the reduced composition after reaction. An ISAT table stores pairs of reduced compositions before and after reaction  $\{\tilde{\mathbf{r}}, \mathbf{R}(\tilde{\mathbf{r}})\}$  together with the gradient matrix  $A_{ij} = \partial f_i / \partial x_j$ , so that given a new query  $\tilde{\mathbf{r}}(t)$  to be evaluated the corresponding value  $\tilde{\mathbf{r}}(t + \Delta t)$  can be retrieved from the table (if it is within the user-specified error tolerance). As needed, pairs of values  $\{\tilde{\mathbf{r}}, \mathbf{R}(\tilde{\mathbf{r}})\}$  are added to the table by the three-step process:

- Given the initial reduced composition  $\tilde{\mathbf{r}}(0)$ , species reconstruction is employed to obtain the initial full composition, denoted by  $\Phi^{\text{CE}}(0) = \{\mathbf{z}^{\text{CE}}, h, p\}$  by assuming that the unrepresented species are in constrained chemical equilibrium.
- The ODEs (see Equation (7)) governing adiabatic, isobaric reaction (according to the given detailed kinetic mechanism) are integrated for a time  $\Delta t$  to obtain the final full composition  $\Phi(\Delta t)$ .
- Then the final reduced composition  $\tilde{\mathbf{r}}(\Delta t)$  is extracted from  $\Phi(\Delta t)$  through Equation (3).

The current three-step implementation is essentially equivalent to that described in [17], except that the more robust constrained equilibrium code CEQ [33] is used. As discussed in [17], since the constrained equilibrium manifold (CEM) is not inertial, the trajectory from Step 2 may depart from the manifold, and consequently the reduced description depends on the reaction time step  $\Delta t$ . An alternative approach for solving the reaction step is to integrate the rate equations for the constraint potentials [16,18], which forces the reduced description on the CEM manifold. It is noted that as the sub-time step  $\Delta t$  approaches zero in solving the equations, the two different implementations will generate the same results and thus are fully consistent with each other. Therefore as the reaction time step  $\Delta t$  approaches zero, the solution of the proposed implementation converges to the reduced description using constrained-equilibrium manifolds, which is an approximation to the full system.

For ISAT tabulation, an important quantity also needed is the gradient matrix  $\mathbf{A}$ , whose components are defined as  $A_{ij} = \partial R_i / \partial \tilde{r}_j$ . According to the three-step ‘add’ procedure, the gradient matrix can be obtained using the chain rule as

$$A_{ij} = \frac{\partial R_i}{\partial \Phi_l(\Delta t)} \frac{\partial \Phi_l(\Delta t)}{\partial \Phi_m^{\text{CE}}(0)} \frac{\partial \Phi_m^{\text{CE}}(0)}{\partial \tilde{r}_j} \quad (9)$$

Notice that the term  $\partial R_i / \partial \Phi_l(\Delta t)$  is related to matrix  $\mathbf{B}$ ; and the ODE sensitivity matrix  $\partial \Phi_l(\Delta t) / \partial \Phi_m^{\text{CE}}(0)$  is readily obtained from the ODE solver DDASAC [35]. The important quantity is the term  $\partial \Phi_m^{\text{CE}}(0) / \partial \tilde{r}_j$  whose columns span the tangent space of the constrained equilibrium manifold. In this study, we have obtained a new, simple expression for it as shown in Appendix 1.

Hence in CFD calculations of reactive flows, the reduction/tabulation approach determines and tabulates, in situ, the necessary information about the  $n_r$ -dimensional reduced system based on the  $n_s$ -species detailed mechanism. Recalling that both the ISAT storage requirement and the retrieval time scale with  $n_x^2$  (with  $n_f \approx n_x$ ). With the reduced description, given the same specified ISAT storage, the ISAT table with  $n_r$  dimensions is capable of covering more of the composition space than the ISAT tabulation of the full  $n_s$  dimensions. Also, the ISAT retrieval is faster than that in the full description. Consequently, a simulation with the reduced description may initially be not much faster than that with full description (due to the extra constrained equilibrium calculations when adding entries in the ISAT table), but iterations can be substantially faster at later times when retrieving from the ISAT table.

#### 4. Implementation in CFD

The reduced description with chemistry tabulation is implemented in the commercial CFD package ANSYS Fluent. It is constructed to work seamlessly with a Chemkin mechanism file with a graphic interface for importing Chemkin mechanisms and specifying the

represented species. ANSYS Fluent solves the conservation equations of mass, momentum, energy and species. One can either specify the transport properties of the notional species to be constants or specify them to be the arithmetic average of those of all the represented species. The thermodynamic properties of the notional species (i.e., the unrepresented elements) are specified to be those of the corresponding species in standard states except for element C, which is specified to be those of gaseous species C(s). (Note that the specification of thermodynamic properties is insignificant if the mixture enthalpy  $h$  is employed to represent energy.)

In the current implementation, the specification of the represented species is obtained as follows. One specifies the number of represented species, as well as some selected represented species such as the fuel and oxidiser species present in the inflowing streams, the major products such as  $\text{CO}_2$  and  $\text{H}_2\text{O}$ , and important intermediate species. (Note that the necessary number of represented species in a reduced representation depends on the level of accuracy required and also on the sensitivity of the phenomena to be captured to chemical kinetics.) The number of user-selected represented species can be less than, but no more than the user-specified input number of represented species  $n_{rs}$ . Next if the number of user-selected represented species is less than the user specified value of  $n_{rs}$ , the solver determines the remaining represented species as follows. First, species  $H$ ,  $OH$ ,  $O$ ,  $H_2$  and  $CO$  are forced to be represented species if they are present in the mechanism and have not been specified to be represented species. Then if the number of selected represented species is still less than the input number of represented species, the remaining represented species are taken from the full mechanism in the order they appear in the Chemkin Mechanism Species list. A more automatic, optimal specification of represented species is described in [34].

## 5. Results

In this study, the reduced description is validated using the following two different tests: a two-dimensional planar stoichiometric  $\text{CH}_4/\text{air}$  premixed flame in a co-flowing air stream and an axi-symmetric opposed-flow  $\text{CH}_4/\text{air}$  non-premixed flame. Both flames are laminar and employ the GRI 1.2 chemical mechanism with four elements, 31 species and 175 reactions [36]. ANSYS Fluent solves the conservation equations of mass, momentum, energy and species with transport properties determined by kinetic theory. Species' diffusivities are calculated by the mixture-averaged formula. The second-order upwind scheme is used for momentum, species and energy with the SIMPLE scheme for pressure-velocity coupling. All calculations are performed with the ISAT error tolerance of  $\varepsilon_{tol} = 10^{-5}$  and with the allowed ISAT table size of 500Mbytes. The ISAT tabulation error at this tolerance was verified to be negligible by comparing with simulations using direct integration. Thus the results from the full description with the ISAT error tolerance  $\varepsilon_{tol} = 10^{-5}$  are regarded to be the exact solutions, and the loss in accuracy of the reduced description is dominantly due to dimension reduction. The loss in accuracy as well as the gain in run-time of the reduced description is reported by comparing against the full description with ISAT. Plots are presented for temperature, and mass fractions of  $CO$ ,  $OH$ , and  $H$ , which are representative of the major species and important intermediate species. The unrepresented species obtained by species reconstruction in the reduced description are also compared to those in the full description.

### 5.1 Two dimensional planar laminar premixed flame

The first test case is a two-dimensional, planar, atmospheric pressure, stoichiometric  $\text{CH}_4/\text{air}$  premixed flame in a co-flowing air stream. The flow configuration is illustrated

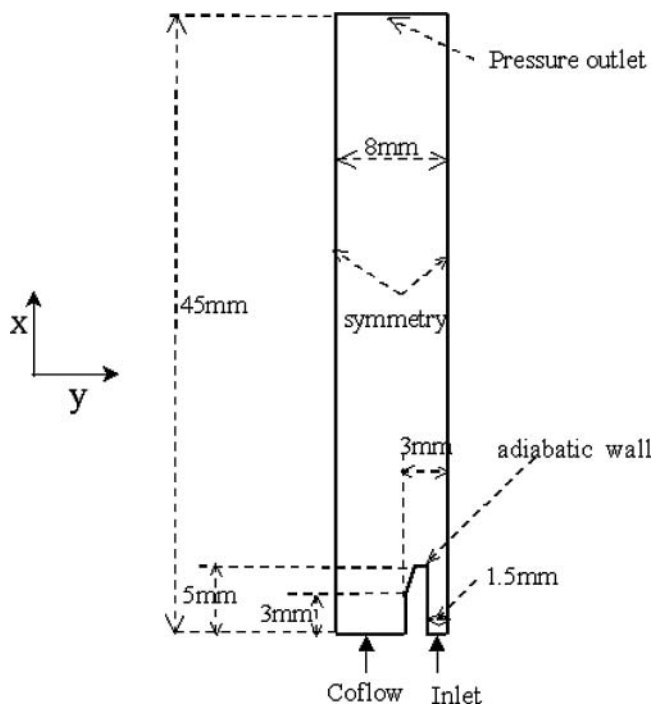


Figure 1. Flow configuration of the two-dimensional planar laminar premixed flame. The boundary conditions of the inlet stream are: the x-component of velocity  $U = 0.6$  m/s; y-component velocity  $V = 0$ ; temperature  $T = 298$  K; mass fraction of species methane  $Y_{\text{CH}_4} = 0.0463$ ;  $Y_{\text{O}_2} = 0.2223$ ;  $Y_{\text{N}_2} = 0.7314$ . The boundary conditions of the co-flow stream are:  $U = 0.05$  m/s;  $V = 0$ ;  $T = 300$  K;  $Y_{\text{O}_2} = 0.22$ ;  $Y_{\text{N}_2} = 0.78$ .

in Figure 1. The mesh consists of about 40,000 cells, which resolves all flame structures adequately. The whole CFD domain is initialised with hot combustion products  $\text{CO}_2$  and  $\text{H}_2\text{O}$  (together with  $\text{N}_2$ ) at 2000 K, with their mass fractions corresponding to complete combustion of the premixed stoichiometric  $\text{CH}_4/\text{air}$  mixture.

Four different reduced descriptions are investigated with the following specifications of the represented species:

- B12-a:  $\text{H}_2, \text{H}, \text{O}, \text{O}_2, \text{OH}, \text{H}_2\text{O}, \text{HO}_2, \text{H}_2\text{O}_2, \text{CH}_4, \text{CO}, \text{CO}_2, \text{N}_2$
- B12-b:  $\text{H}_2, \text{H}, \text{O}, \text{O}_2, \text{OH}, \text{H}_2\text{O}, \text{CH}_3, \text{CH}_4, \text{CO}, \text{CO}_2, \text{CH}_2\text{O}, \text{N}_2$
- B16-a:  $\text{H}_2, \text{H}, \text{O}, \text{O}_2, \text{OH}, \text{H}_2\text{O}, \text{HO}_2, \text{H}_2\text{O}_2, \text{C}, \text{CH}, \text{CH}_2, \text{CH}_2(\text{s}), \text{CH}_4, \text{CO}, \text{CO}_2, \text{N}_2$
- B16-b:  $\text{H}_2, \text{H}, \text{O}, \text{O}_2, \text{OH}, \text{H}_2\text{O}, \text{HO}_2, \text{H}_2\text{O}_2, \text{CH}_3, \text{CH}_4, \text{CO}, \text{CO}_2, \text{CH}_2\text{O}, \text{C}_2\text{H}_4, \text{C}_2\text{H}_6, \text{N}_2$

For this case, the element  $N$  is fully represented by the species  $\text{N}_2$ , and the unrepresented elements  $C$ ,  $H$  and  $O$  are considered as notional species denoted as  $UC$ ,  $UH$ , and  $UO$  respectively.

The reduced representations B12-a and B16-a are obtained by specifying the fuel species  $\text{CH}_4$ , the oxidiser species  $\text{O}_2$ , the major product species  $\text{H}_2\text{O}$  and  $\text{CO}_2$ , and the intermediate species  $\text{H}$ ,  $\text{OH}$ ,  $\text{O}$ ,  $\text{H}_2$  and  $\text{CO}$ . The remaining represented species are determined by the order in which they appear in the full mechanism. In contrast, the represented species in

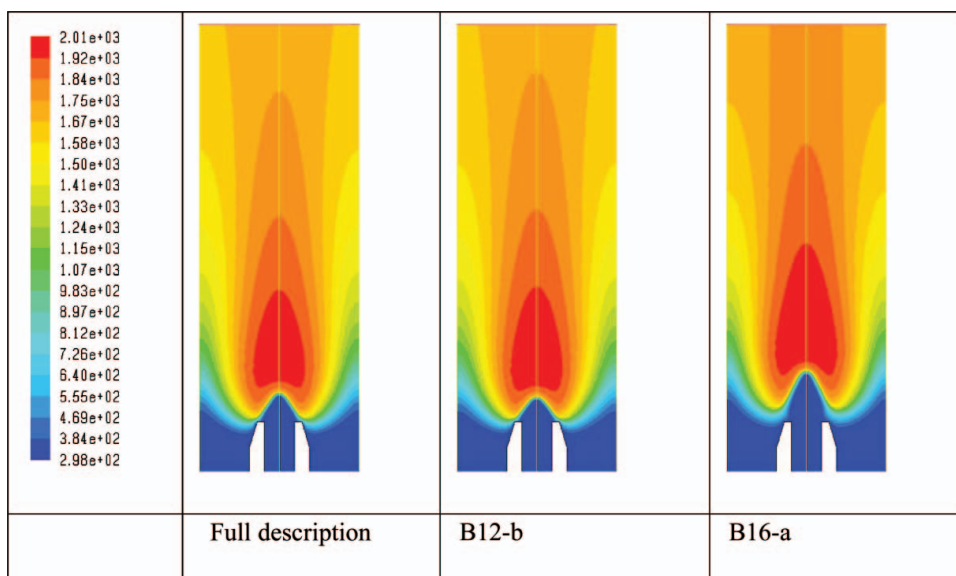


Figure 2. Contour plots of temperature (K) from the two-dimensional planar laminar premixed flame. Left: full description; middle: B12-b; right: B16-a.

B12-b and B16-b are manually chosen to include the important species in the main reaction pathway, such as  $CH_3$  and  $CH_2O$ .

Figures 2–4 show the contour plots of temperature,  $CO$  and  $OH$  from both the full and reduced descriptions. It is observed that B12-a cannot establish a flame because it does

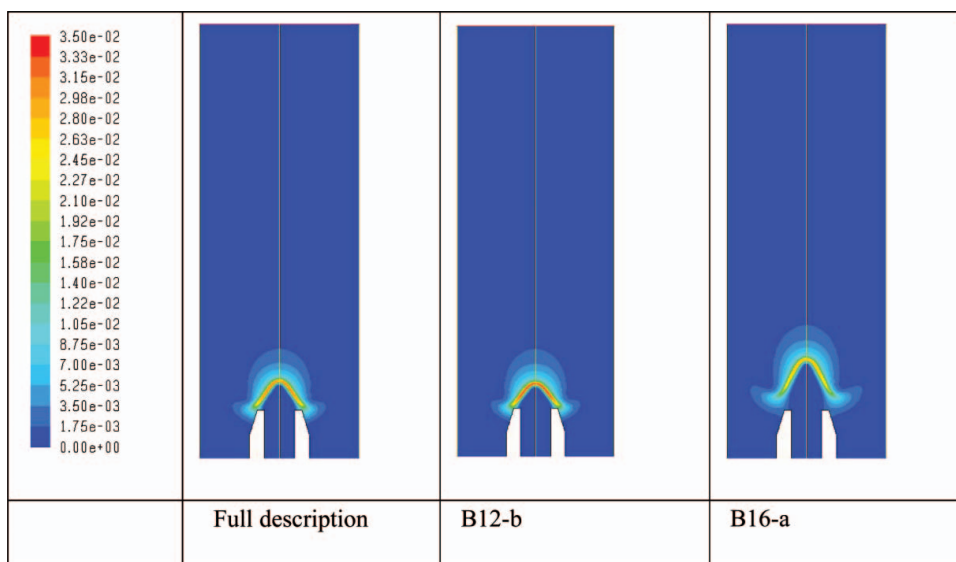


Figure 3. Contour plots of mass fraction of  $CO$  from the two-dimensional planar laminar premixed flame. Left: full description; middle: B12-b; right: B16-a.

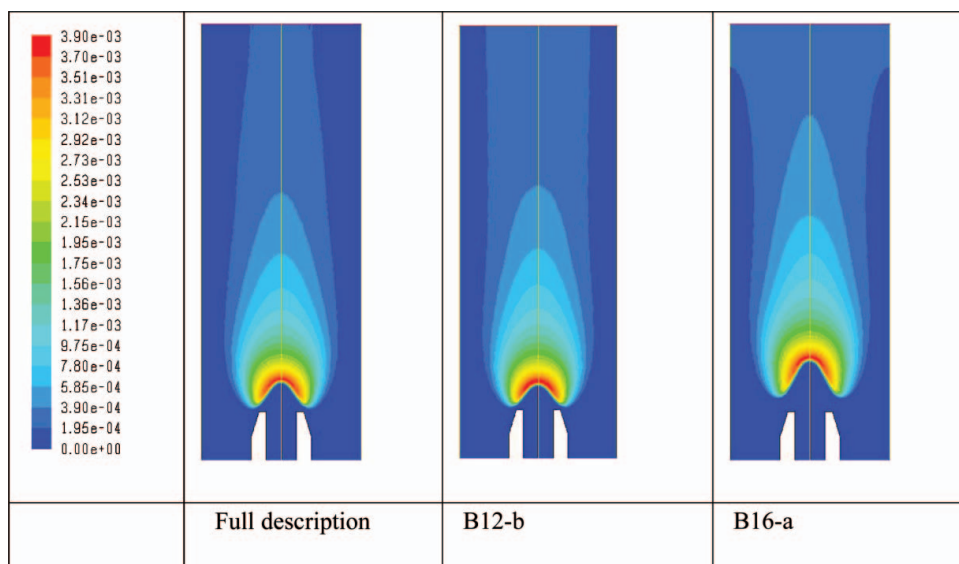


Figure 4. Contour plots of mass fraction of  $OH$  from the two-dimensional planar laminar premixed flame. Left: full description; middle: B12-b; right: B16-a.

not include enough carbon-containing intermediate species in the represented species and consequently cannot accurately capture the flame. By increasing the number of represented species, as shown in the figure, B16-a with the additional  $C$ ,  $CH$ ,  $CH_2$ ,  $CH_2(s)$  represented species yields a stable flame, which in general is in agreement with the full description predictions. More interestingly, B12-b with 12 represented species gives a more accurate reduced description than B16-a as far as the flame location is concerned. This clearly illustrates the significance of a prior knowledge of chemical kinetics which helps achieve a good quality of reduced description with a minimum number of represented species or the need for an automatic method as studied in [34]. As demonstrated, for this premixed laminar flame, the specification of represented species is critical. Without prior knowledge of chemical kinetics, an alternative approach to improve the accuracy of the reduced description is to increase the number of represented species.

A quantitative comparison between full and reduced descriptions is given in Figures 5–7, which show the profiles of temperature,  $CO$  and  $OH$  along the centre line. In these plots, represented species B12-b and B16-b give better predictions of the flame location compared to B16-a. The centre line flame location of B16-a is substantially shifted downstream, which implies a smaller laminar flame speed. The accuracy of B12-b and B16-b is comparable, and the inclusion of the four species  $HO_2$ ,  $H_2O_2$ ,  $C_2H_4$  and  $C_2H_6$  does not improve the accuracy of the reduced description. The additional four species shift the flame location slightly downstream. Again, this illustrates the need for a method for optimal selection of the represented species [34].

The distribution of the unrepresented elements (treated as notional species) is shown in Figure 8. Two important observations are as follows. The unrepresented elements are small in quantity. As shown for B16-b, the peak value of the mass fraction of the largest unrepresented element (carbon) is less than 0.002, which is less than 5% of the value of carbon at fuel inlet. (Notice that the mass fraction of methane at fuel inlet is  $Y_{CH_4}^f = 0.046$ .)

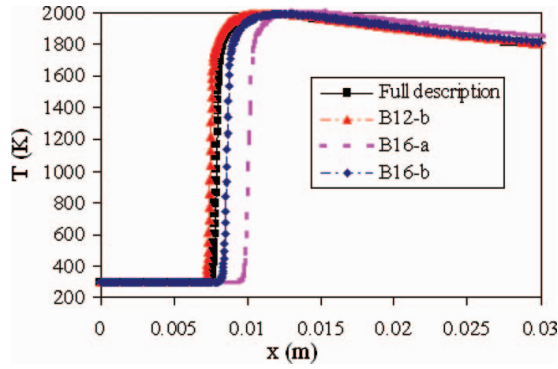


Figure 5. Temperature along the centre line of the two-dimensional planar laminar premixed flame.

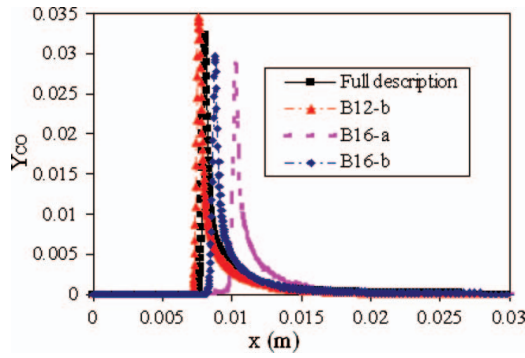


Figure 6. Mass fraction of CO along the centre line of the two-dimensional planar laminar premixed flame.

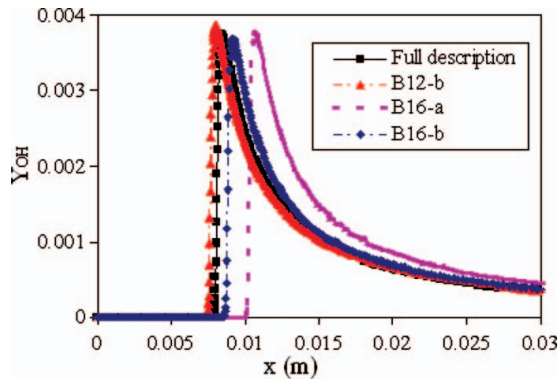


Figure 7. Mass fraction of OH along the centre line of the two-dimensional planar laminar premixed flame.

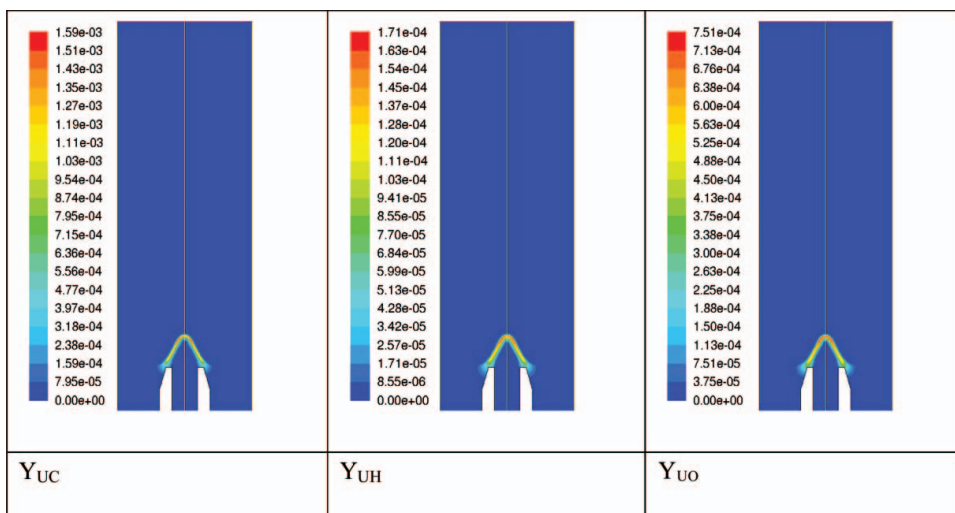


Figure 8. Contour plot of the mass fractions of the notional species, i.e., unrepresented elements in the reduced description of B16-b.

The unrepresented elements are localised in the flame front region. For all other regions, they are close to zero since all the elements exist in the major reactants or products.

In this study, we have also studied the effect of different specifications of transport properties for the unrepresented elements. The transport properties for the unrepresented elements  $UC$ ,  $UH$ , and  $UO$  have been specified to be those of  $H_2$ ,  $N_2$  or the arithmetic average of all the represented species. No noticeable difference has been observed in the

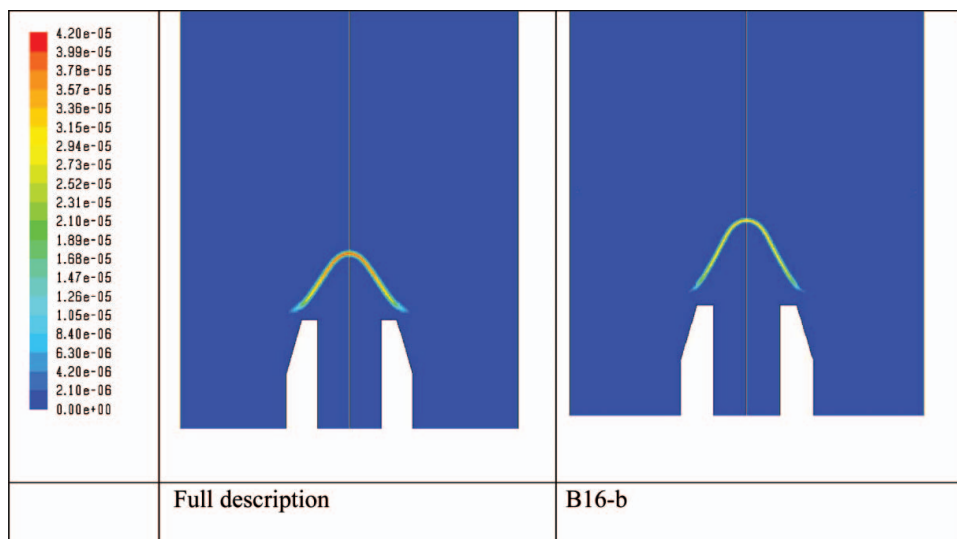


Figure 9. Contour plot of mass fraction of  $HCO$ . In the reduced description of B16-b,  $HCO$  is an unrepresented species.

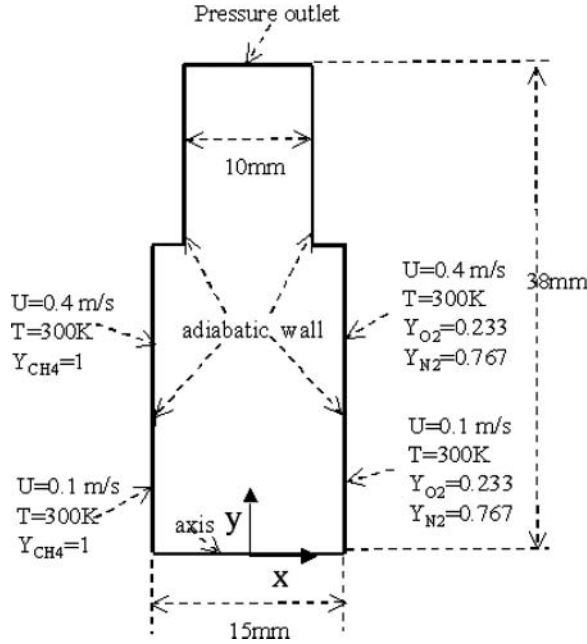


Figure 10. Flow configuration and boundary conditions of the two-dimensional axis-symmetric laminar diffusion flame.

reduced description with different specifications, which is partly due to the low concentration of the unrepresented elements.

As described in Section 2.1, the unrepresented species in the reduced description can be reconstructed, when needed, assuming that they are in constrained chemical equilibrium.

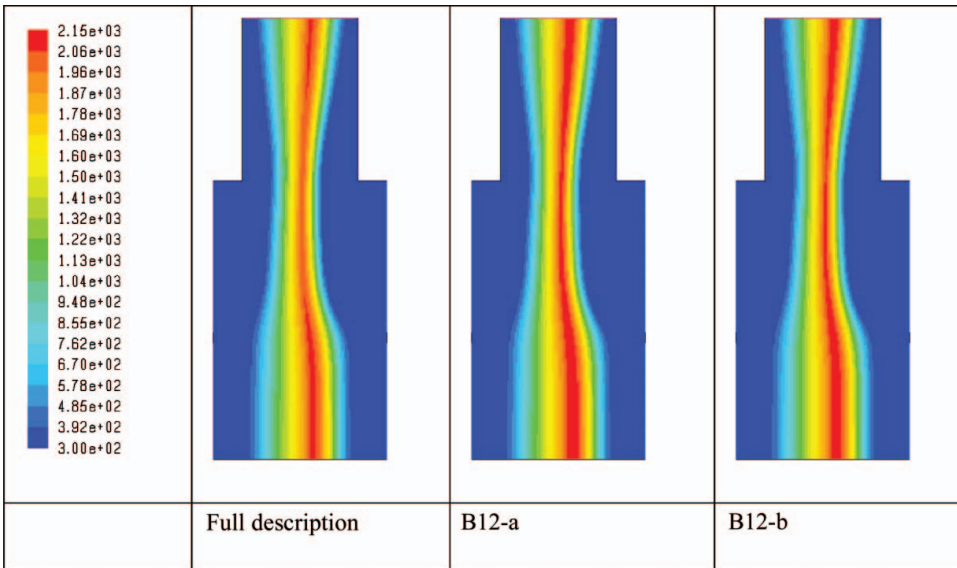


Figure 11. Contour plots of temperature (K) from the two-dimensional axis-symmetric laminar non-premixed flame. Left: full description; middle: B12-a; right: B12-b.

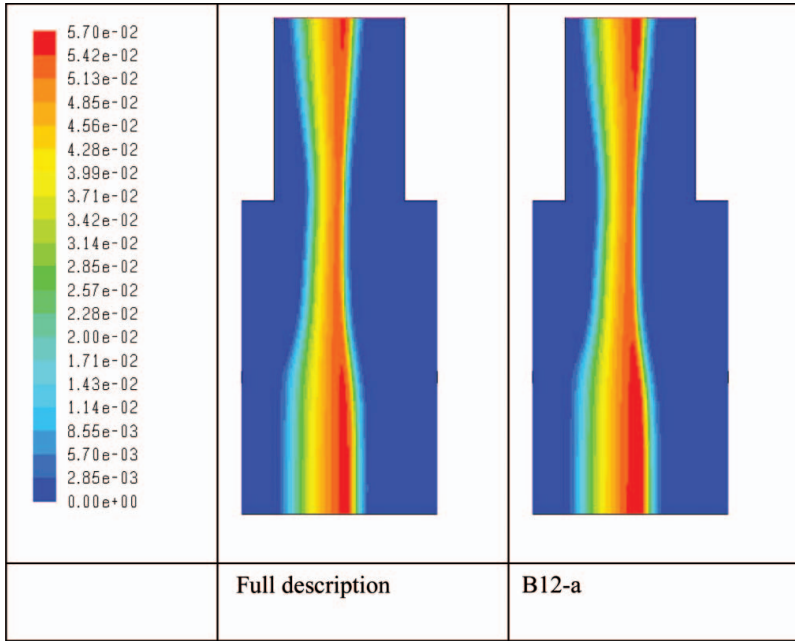


Figure 12. Contour plots of mass fraction of  $CO$  from the two-dimensional axi-symmetric laminar non-premixed flame. Left: full description; right: B12-a.

Figure 9 shows the mass fraction of  $HCO$  from both the full and reduced descriptions. (The species  $HCO$  is an unrepresented species in all reduced descriptions.) The difference in peak value is within 30%. For some other unrepresented species, even larger differences have been observed. This implies that a large error in the unrepresented species may not

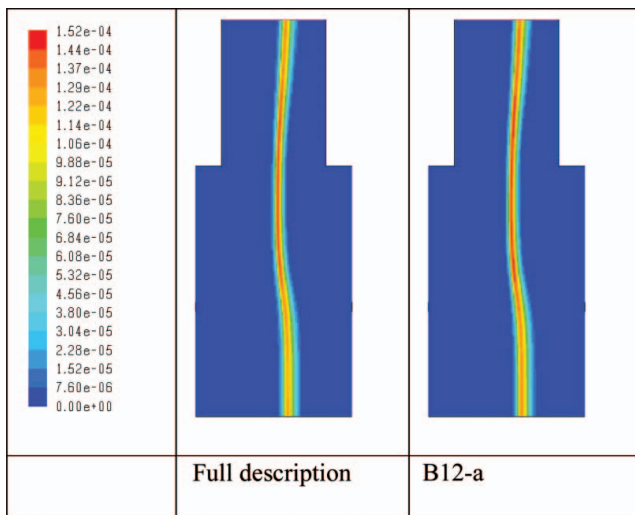


Figure 13. Contour plot of mass fraction of  $H$  from the two-dimensional axi-symmetric laminar non-premixed flame. Left: full description; right: B12-a.

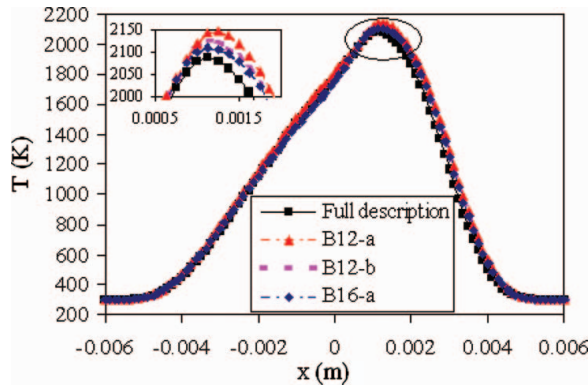


Figure 14. Temperature along the axis from the two-dimensional axi-symmetric laminar non-premixed flame.

necessarily have a significant effect on the represented species of concern. In the present reduced species description method, the reconstructed full composition is only used as the initial condition to the full set of ODEs governing the reaction fractional step. Due to the wide range of chemical time scales, all solution trajectories from different initial conditions quickly relax toward the intrinsic low dimensional attracting manifold. Hence the effect of any inaccuracy in the initial condition is likely to be quickly damped out during the reaction fractional step if the unrepresented species are associated with the fast time scales.

## 5.2 Axi-symmetric laminar non-premixed flame

The second test case is an axi-symmetric, laminar opposed-flow non-premixed flame. The fuel jet is pure methane at a temperature of 300 K, the oxidiser jet is air at a temperature of 300 K, and the pressure is one atmosphere. The global strain rate, defined as the fuel velocity magnitude, plus the air velocity magnitude, divided by the distance between the jets, is  $13\text{s}^{-1}$ . The flow configuration is illustrated in Figure 10. The mesh consists of 32000

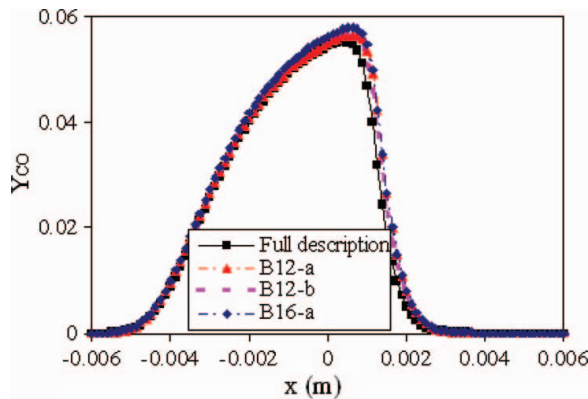


Figure 15. Mass fraction of species  $CO$  along the axis from the two-dimensional axi-symmetric laminar non-premixed flame.

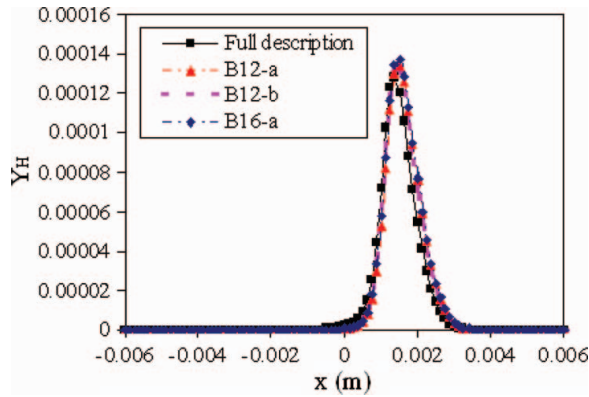


Figure 16. Mass fraction of species  $H$  along the axis from the two-dimensional axi-symmetric laminar non-premixed flame.

CFD cells, which resolves all flame structures. The whole CFD domain is initialised with hot combustion products  $CO_2$  and  $H_2O$  (together with  $N_2$ ) at 2000 K, with their mass fractions corresponding to complete combustion of stoichiometric  $CH_4$ /air mixture.

For this test, the three different reduced descriptions B12-a, B12-b and B16-a are performed (see Section 5.1 for details of the represented species). The unrepresented elements  $C$ ,  $H$  and  $O$  are again considered as notional species denoted as  $UC$ ,  $UH$ , and  $UO$ , respectively.

Figures 11–13 show the contour plots of temperature,  $CO$  and  $OH$  from both the full and reduced descriptions. It can be seen that for this case, even B12-a is in good agreement with the full description, although the peak flame temperature is over-predicted by about 60 K. For this non-premixed flame, the specification of represented species is not as critical as

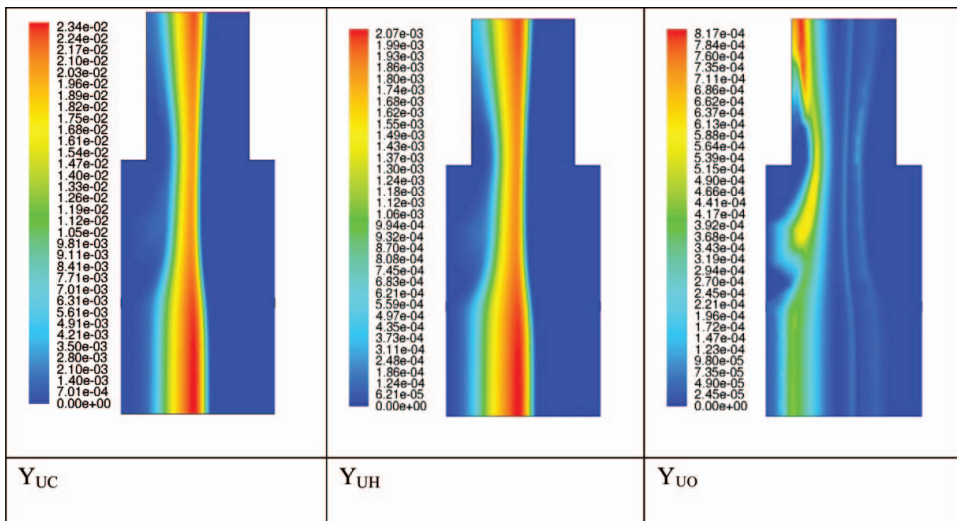


Figure 17. Contour plot of mass fractions of the notional species, i.e., unrepresented elements in the reduced description B12-b.

Table 1. The wall clock time (in seconds) per iteration for different runs.

	Full description	B12-a	B12-b	B16-a	B16-b
Premixed flame	11	X	6.2	7.4	7.2
Non-premixed flame	9.5	4.5	3.8	5.2	X

for the premixed flame shown in the previous section. This is expected since non-premixed flames (away from extinction) are mainly controlled by diffusion process, whereas for premixed flames both chemical kinetics and transport processes are important. As shown, the flame predicted by B12-b is very similar to the B12-a with a slightly better agreement with the full description. The over-prediction in peak temperature decreases from about 60 K in B12-a to about 40 K in B12-b.

A quantitative comparison between full and reduced descriptions is given in Figures 14–16, which show profiles of temperature,  $CO$  and  $H$  along the axis. All reduced descriptions are in good agreement with the full description. By increasing the number of represented species, as shown in Figure 14, B16-a with the additional  $C$ ,  $CH$ ,  $CH_2$ ,  $CH_2(s)$  represented species yields a more accurate prediction. The distribution of the unrepresented elements (treated as notional species) is shown in Figure 17. Similar to the premixed flame, the unrepresented elements are small in quantity. As shown for B12-b, the peak value of the mass fraction of the largest unrepresented element (carbon) is less than 0.02. The unrepresented elements are localised in the fuel rich region, where certain hydrocarbon radicals are not represented. For the unrepresented element  $O$  that has the lowest concentration among the unrepresented elements, a non-smooth distribution is observed. This is caused by numerical errors such as ISAT tabulation error.

In this study, all the flame calculations require about 20,000 iterations to converge. With the use of ISAT, the full description has already achieved a speed-up factor of about 20 for the non-premixed flame and 50 for the premixed flame compared to the ones without ISAT. (This modest speed-up is due to the fact that an excessively small ISAT error tolerance  $\varepsilon_{tol} = 1 \times 10^{-5}$  is used in this study to make sure that the ISAT tabulation error is negligible.) Compared to the full description with ISAT, the reduced descriptions can potentially achieve additional computational speed-up by solving fewer transport equations and faster ISAT retrieving. As shown in Table 1, for all the long-run calculations, the reduced descriptions exhibit a speed-up factor of up to 2.5 compared to the full description with ISAT.

## 6. Conclusion

In this study, a reduced description of reactive flows in combination with chemistry tabulation is proposed to effectively reduce the computational burden imposed by the use of a large chemical mechanism in CFD. In the reduced description, the full set of chemical species in the mechanism is partitioned into represented species and unrepresented species; the reactive system is described in terms of a smaller number of reduced compositions consisting of represented species and the elements in the unrepresented species, and the evolution equations are solved for only the reduced composition. With specified thermal and transport properties, the elements in the unrepresented species are treated as notional species with corresponding PDEs governing the evolution.

The current approach employs operator splitting to separate chemical reaction process into a reaction fractional step, where ISAT is used to accelerate the determination of

the reduced composition after reaction by tabulating combustion chemistry into an ISAT table. During the reaction fractional step, when required, the unrepresented species are reconstructed assuming that they are in constrained chemical equilibrium.

The reduced description with chemistry tabulation is implemented in the commercial CFD package ANSYS Fluent with a graphic interface for importing Chemkin mechanisms and specifying the represented species. It has been applied to two-dimensional steady premixed and non-premixed  $CH_4$ /air flames. Studies show that the specification of represented species is critical to the accuracy of the reduced description for premixed flames, but less critical for diffusion flames. Without prior knowledge of chemical kinetics, one effective way to improve the accuracy of the reduced description is to increase the number of represented species. For both flames, with 12 represented species, the reduced description can achieve good agreement with the full description involving 31 species.

If the represented species include the major reactant and product species, important radicals and the intermediate species with large concentration, then as demonstrated, the unrepresented elements are small on quantity. Consequently, no noticeable difference has been observed in the reduced description with different specifications of thermal-transport properties for the unrepresented species.

Compared to the full description with ISAT, the reduced descriptions achieve additional computational speed-up by solving fewer transport equations and faster ISAT retrieving. In this study, with the relatively small GRI 1.2 mechanism consisting of 31 species, the reduced descriptions (with 12 to 16 represented species) achieve a speed-up factor of up to three compared to the full description with ISAT.

### Acknowledgements

Ren and Goldin are grateful to the financial support of the Austrian Kplus programme funded by the Federal Government of Austria as well as the State Governments of federal states of Styria and Lower Austria. The work at Cornell is funded in part by Department of Energy under Grant DE-FG02-90ER. SBP has a financial interest in Ithaca Combustion Enterprise, LLC, which has licensed the software ISAT-CK and CEQ used in this work.

### References

- [1] C.K. Law, *Combustion at a crossroads: Status and prospects*, Proc. Combust. Inst. 31 (2007), pp. 1–29.
- [2] H.J. Curran, P. Gaffuri, W.J. Pitz, and C.K. Westbrook, *A comprehensive modeling study of iso-octane oxidation*, Combust. Flame 129 (2002), pp. 253–280.
- [3] J.F. Griffiths, *Reduced kinetic models and their application to practical combustion systems*, Prog. Energy Combust. Sci. 21 (1995), pp. 25–107.
- [4] A.S. Tomlin, T. Turányi, and M.J. Pilling, *Comprehensive chemical kinetics 35*, in *Low-temperature Combustion and Autoignition*, M.J. Pilling, ed., Elsevier, Amsterdam, 1997, pp. 293–437.
- [5] M.S. Okino and M.L. Mavrouniotis, *Simplification of mathematical models of chemical reaction systems*, Chem. Rev. 98 (1998), pp. 391–408.
- [6] T. Lu and C.K. Law, *Toward accommodating realistic fuel chemistry in large-scale computations*, Prog. Energy Combust. Sci. 35 (2009), pp. 192–215.
- [7] S.B. Pope and Z. Ren, *Efficient implementation of chemistry in computational combustion*, Flow Turbul. Combust. 82 (2009), pp. 437–453.
- [8] G.M. Goldin, Z. Ren, and S. Zahirovic, *A cell agglomeration algorithm for accelerating detailed chemistry in CFD*, Combust. Theory Model. 13 (2009), pp. 721–739.
- [9] T. Lu and C.K. Law, *A directed relation graph method for mechanism reduction*, Proc. Combust. Inst. 30 (2005), pp. 1333–1341.

- [10] M. Valorani, F. Creta, D.A. Goussis, J.C. Lee, and H.N. Najm, *An automatic procedure for the simplification of chemical kinetic mechanisms based on CSP*, *Combust. Flame* 146 (2006), pp. 29–51.
- [11] P. Pepiot and H. Pitsch, *An efficient error-propagation-based reduction method for large chemical kinetic mechanisms*, *Combust. Flame* 154 (2008), pp. 67–81.
- [12] M. Bodenstein and S.C. Lind, *Geschwindigkeit der bildung des bromwasserstoffs aus seinen elementen*, *Z Phys. Chem.* 57 (1906), pp. 168–175.
- [13] M.D. Smooke (ed.), *Reduced Kinetic Mechanisms and Asymptotic Approximations for Methane-Air Flames*, Vol. 384, Springer, Berlin, 1991.
- [14] J.-Y. Chen, *A general procedure for constructing reduced reaction mechanisms with given independent relation*, *Combust. Sci. Technol.* 57 (1988), pp. 89–94.
- [15] J.C. Keck and D. Gillespie, *Rate-controlled partial equilibrium method for treating reacting gas-mixtures*, *Combust. Flame* 17 (1971), pp. 237–241.
- [16] J.C. Keck, *Rate-controlled constrained equilibrium theory of chemical reactions in complex systems*, *Prog. Energy Combust. Sci.* 16 (1990), pp. 125–154.
- [17] Q. Tang and S.B. Pope, *Implementation of combustion chemistry by in situ adaptive tabulation of rate-controlled constrained equilibrium manifolds*, *Proc. Combust. Inst.* 29 (2002), pp. 1411–1417.
- [18] Q. Tang and S.B. Pope, *A more accurate projection in the rate-controlled constrained equilibrium method for dimension reduction of combustion chemistry*, *Combust. Theory Model.* 8 (2004), pp. 255–279.
- [19] W.P. Jones and S. Rigopoulos, *Rate-controlled constrained equilibrium: Formulation and application to nonpremixed laminar flames*, *Combust. Flame* 142 (2005), pp. 223–234.
- [20] M. Janbozorgi, S. Ugarte, H. Metghalchi, and J.C. Keck, *Combustion modeling of mono-carbon fuels using the rate-controlled constrained-equilibrium method*, *Combust. Flame* 156 (2009), pp. 1871–1885.
- [21] A.N. Gorban and I.V. Karlin, *Method of invariant manifold for chemical kinetics*, *Chem. Eng. Sci.* 58 (2003), pp. 4751–4768.
- [22] U. Maas and S.B. Pope, *Simplifying chemical-kinetics: Intrinsic low-dimensional manifolds in composition space*, *Combust. Flame* 88 (1992), pp. 239–264.
- [23] S.B. Pope and U. Maas, *Simplifying chemical kinetics: Trajectory-generated low-dimensional manifolds*, FDA 93-11, Cornell University, USA, 1993.
- [24] Z. Ren, S.B. Pope, A. Vladimirov, and J.M. Guckenheimer, *The invariant constrained equilibrium edge preimage curve method for the dimension reduction of chemical kinetics*, *J Chem. Phys.* 124 (2006), p. 114111.
- [25] S.H. Lam, *Using CSP to understand complex chemical kinetics*, *Combust. Sci. Technol.* 89 (1993), pp. 375–404.
- [26] S.H. Lam and D.A. Goussis, *The CSP method for simplifying kinetics*, *Int. J. Chem. Kinet.* 26 (1994), pp. 461–486.
- [27] T. Lu, Y. Ju, and C.K. Law, *Complex CSP for chemistry reduction and analysis*, *Combust. Flame* 126 (2001), pp. 1445–1455.
- [28] S.B. Pope, *Computationally efficient implementation of combustion chemistry using in situ adaptive tabulation*, *Combust. Theory Model.* 1 (1997), pp. 41–63.
- [29] L. Lu and S.B. Pope, *An improved algorithm for in situ adaptive tabulation*, *J Comput. Phys.* 228 (2009), pp. 361–386.
- [30] Q. Tang, J. Xu, and S.B. Pope, *PDF calculations of local extinction and NO production in piloted-jet turbulent methane/air flames*, *Proc. Combust. Inst.* 28 (2000), pp. 133–139.
- [31] Z. Ren and S.B. Pope, *Species reconstruction using pre-image curves*, *Proc. Combust. Inst.* 30 (2005), pp. 1293–1300.
- [32] Z. Ren and S.B. Pope, *Entropy production and element conservation in the quasi-steady-state approximation*, *Combust. Flame* 137 (2004), pp. 251–254.
- [33] S.B. Pope, *Gibbs function continuation for the stable computation of chemical equilibrium*, *Combust. Flame* 139 (2004), pp. 222–226.
- [34] V. Hiremath, Z. Ren, and S.B. Pope, *A greedy algorithm for species selection in dimension reduction of combustion chemistry*, *Combust. Theory Model.* 14 (2010), pp. 619–652.
- [35] M. Caracotsios and W.E. Stewart, *Sensitivity analysis of initial-value problems with mixed ODEs and algebraic equations*, *Comput. Chem. Eng.* 9 (1985), pp. 359–365.

- [36] M. Frenklach, H. Wang, M. Goldenberg, G.P. Smith, D.M. Golden, C.T. Bowman, R.K. Hanson, W.C. Gardiner, and V. Lissianski, *GRI-Mech: An optimized detailed chemical reaction mechanism for methane combustion*, Gas Research Institute topical report, Gas Research Institute, Chicago, 1995.

### Appendix 1. The tangent vectors of the constrained equilibrium manifold

In the following, we derive a new simple expression for the matrix  $\partial\Phi_m^{\text{CE}}/\partial\tilde{r}_j$  whose columns span the tangent space of the constrained equilibrium manifold. For simplicity of exposition, it is presented here for the case of fixed pressure and temperature, from which the corresponding result with fixed  $p$  and  $h$  is readily obtained.

Let the columns of the  $n_s \times n_r$  matrix  $\mathbf{T}^{\text{CE}}$  span the tangent space of the CE manifold. It relates infinitesimal changes in  $\mathbf{z}^{\text{CE}}$  to those in  $\mathbf{r}$  by

$$d\mathbf{z}^{\text{CE}} = \mathbf{T}^{\text{CE}}d\mathbf{r} \tag{10}$$

For the case considered, the constrained equilibrium composition is given by [33]

$$\mathbf{z}^{\text{CE}} = \bar{N} \exp(-\tilde{\mathbf{g}} + \mathbf{B}\boldsymbol{\lambda}) \tag{11}$$

where  $\bar{N} = \sum_{i=1}^{n_s} z_i^{\text{CE}}$  is the specific moles of all species;  $\tilde{\mathbf{g}}$  are normalised Gibbs functions; and  $\boldsymbol{\lambda}$  are constraint potentials (or Lagrange multipliers). Considering infinitesimals, we obtain from Equation (11)

$$d\mathbf{z}^{\text{CE}} = \mathbf{z}^{\text{CE}}d\ln(\bar{N}) + \mathbf{ZB}d\boldsymbol{\lambda} \tag{12}$$

where  $\mathbf{Z}$  is the diagonal matrix formed from  $\mathbf{z}^{\text{CE}}$  (i.e., the diagonal components of matrix  $\mathbf{Z}$  are taken to be the components of vector  $\mathbf{z}^{\text{CE}}$ ). Summing Equation (12) over all the species leads to the constraint

$$0 = \mathbf{z}^T \mathbf{B}d\boldsymbol{\lambda} = \mathbf{r}^T d\boldsymbol{\lambda} \tag{13}$$

Equation (12) can be re-expressed as

$$d\mathbf{z}^{\text{CE}} = \mathbf{M}d\hat{\boldsymbol{\lambda}} \tag{14}$$

with

$$d\hat{\boldsymbol{\lambda}} \equiv d\boldsymbol{\lambda} + \frac{rd\bar{N}}{|\mathbf{r}|^2 \bar{N}} \tag{15}$$

and

$$\mathbf{M} \equiv \mathbf{z}\mathbf{r}^T + \mathbf{ZB}\left(\mathbf{I} - \frac{\mathbf{r}\mathbf{r}^T}{|\mathbf{r}|^2}\right) \tag{16}$$

We observe from Equation (14) that the columns of  $\mathbf{M}$  span the tangent space. Let  $\mathbf{W}$  denote any  $n_s \times n_r$  matrix with  $\text{span}(\mathbf{W}) = \text{span}(\mathbf{M}) = \text{span}(\mathbf{T}^{\text{CE}})$ . Then there exists a

non-singular  $n_r \times n_r$  matrix  $\mathbf{D}$  such that  $\mathbf{T}^{\text{CE}} = \mathbf{W}\mathbf{D}$ . From Equation (3) we obtain

$$\mathbf{B}^T dz^{\text{CE}} = d\mathbf{r} = \mathbf{B}^T \mathbf{T}^{\text{CE}} d\mathbf{r} = \mathbf{B}^T \mathbf{W}\mathbf{D}d\mathbf{r} \quad (17)$$

and hence

$$\mathbf{B}^T \mathbf{T}^{\text{CE}} = \mathbf{I} \quad (18)$$

$$\mathbf{D} = (\mathbf{B}^T \mathbf{W})^{-1} \quad (19)$$

and finally

$$\mathbf{T}^{\text{CE}} = \mathbf{W}(\mathbf{B}^T \mathbf{W})^{-1} \quad (20)$$

It is interesting to observe that  $\mathbf{T}^{\text{CE}}$  is solely determined by  $\mathbf{z}^{\text{CE}}$  and  $\mathbf{B}$ , and does not otherwise depend on any thermodynamic information (such as  $p$ ,  $T$  or  $\tilde{\mathbf{g}}$ ).

In practice  $\mathbf{W}$  is best taken as an orthonormal basis for  $\text{span}(\mathbf{T}^{\text{CE}})$ , obtained from the singular value decomposition or QR decomposition of  $\mathbf{M}$ . The current formulation allows a more robust calculation of the CEM tangent vectors compared to that in [17].